Technical Sciences
Academy of Romania
www.jesi.astr.ro

Journal of Engineering Sciences and Innovation
Volume 4, Issue 3 / 2019, pp. 115 - 130

A. Mechanical Engineering

Received ***4 February 2019*** *Accepted* ***30 May 2019***
Received in revised from ***6 May 2019***

Modal analysis of a simple cyclic system

MIRCEA RADEŞ[*]

Strength of Materials Department, Politehnica University of Bucharest,
Splaiul Independenţei 313, Bucharest, Romania

Abstract. Cyclic systems have double modes with identical natural frequencies. Using the theory of circulants, independent eigenvectors can be exactly determined without slightly perturbing the eigenvalues. The paper presents the contribution of the double modes to the frequency response functions (FRFs) of cyclic systems with proportional damping. The mode indicator functions UMIF and CoMIF, based on the left singular vectors of a matrix encompassing all available FRFs as columns, are applied to simulated noise-free data. It is shown that they can reveal double modes even using FRFs from single point excitation.

Keywords: cyclic structures, circulant matrices, double modes, mode indicator functions.

1. Introduction

Axisymmetric and cyclically periodic structures possess pairs of modes with identical natural frequencies (repeated roots, degenerate modes). *Double* modes are orthogonal, having identical modal shapes but rotated relatively. Any combination of such two modes is also a mode shape.
Cyclically periodic structures are described by *circulant matrices*. The eigenvalues of a circulant matrix can be exactly determined even if they are double. The eigenvectors of all circulant matrices of the same order are the same.
Structures with small deviations from cyclic symmetry possess double modes with *split* natural frequencies. They are coupled by the inherent structural damping and generally cannot be detected in a measured response function where the peaks are merged in the neighbourhood of a resonance. It is difficult to estimate the system order, i.e. the number of dominant modes in a given frequency range. One has to use data from more than one reference.
In order to obtain independent eigenvectors it is customary to desymmetrize a cyclic system by introducing an imperfection in the cyclic symmetry. The structure

[*]Correspondence address: rades@accessmedia.ro

is slightly perturbed by adding (or removing) a small mass (or stiffness) at a given location. In such *quasi-periodic* structures, double modes are split into pairs of closed modes, usually with merged peaks in the response curves but with distinct peaks in the mode indicator functions.

2. Lumped parameter cyclic system

Consider the system shown in Fig. 1 [1]. It consists of a set of N identical light cantilevers, each of stiffness k, and carrying a mass m at their ends. The masses are coupled by springs of stiffness s. The radial cantilevers are uniformly clamped around a circular stationary rigid hub.
The dynamics of the system is defined by the transverse displacements x_q $(q = 0, \dots, N-1)$ of the lumped masses.
Note that the numbering is clockwise and starts with the upper mass.
Four systems will be considered in the following: a) the *Undamped Tuned System*, b) the *Undamped Mass-Mistuned System*, with a single lumped mass added to an existing mass, c) the *Damped Tuned System*, with proportional damping added to the cantilevers and the coupling springs, to simulate realistic frequency response curves, and d) the *Damped Mistuned System*, with added mass and proportional damping.

2.1. Undamped tuned system

The equation of motion for a typical mass is

$$m\ddot{x}_q + kx_q + s\left(2x_q - x_{q+1} - x_{q-1}\right) = 0 \tag{1}$$

or

$$\ddot{x}_q - \frac{s}{m}x_{q-1} + \left(\frac{k}{m} + \frac{2s}{m}\right)x_q - \frac{s}{m}x_{q+1} = 0. \tag{1.a}$$

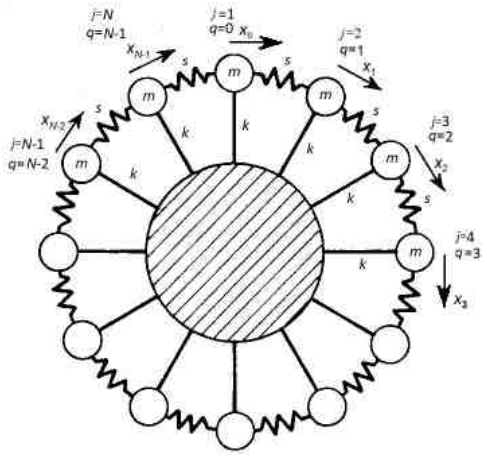

Fig. 1. Lumped parameter cyclic system.

The cyclic boundary conditions are

$$x_0 = x_N, \quad x_{-1} = x_{N-1} \quad (\text{or } x_1 = x_{N+1}). \tag{2}$$

In matrix form, the equations of free motion can be written

$$[m]\{\ddot{x}\} + [k]\{x\} = \{0\} \tag{3}$$

where the diagonal mass matrix is

$$[m] = \text{diag}(m) = m[I] \tag{4}$$

and the real symmetric stiffness matrix is

$$[k] = \begin{bmatrix} k+2s & -s & 0 & \cdots & 0 & -s \\ -s & k+2s & -s & \cdots & 0 & 0 \\ 0 & -s & k+2s & \cdots & 0 & 0 \\ \cdots & \cdots & \cdots & \vdots & \cdots & \cdots \\ 0 & 0 & 0 & \cdots & k+2s & -s \\ -s & 0 & 0 & \cdots & -s & k+2s \end{bmatrix}. \tag{5}$$

The vector of displacements is

$$\{x\} = \{x_0 \quad x_1 \quad \ldots \quad x_q \quad \ldots \quad x_{N-1}\}^T. \tag{6}$$

The eigenvalues ω_p^2 and the eigenvectors $\{X\}_p$ are solutions of

$$[C]\{X\} = \omega^2\{X\} \tag{7}$$

where

$$[C]=[m]^{-1}[k] = \text{circ}\left(\frac{k+2s}{m}, \quad -\frac{s}{m}, \quad 0, \quad \ldots, \quad 0, \quad -\frac{s}{m}\right) \tag{8}$$

is a real symmetric circulant matrix [2] of the form

$$[C] = \begin{bmatrix} c_0 & c_1 & 0 & \cdots & 0 & c_{N-1} \\ c_{N-1} & c_0 & c_1 & 0 & 0 & 0 \\ 0 & c_{N-1} & c_0 & c_1 & 0 & 0 \\ \cdots & \cdots & \cdots & \vdots & \cdots & \cdots \\ 0 & 0 & 0 & \ldots & c_0 & c_1 \\ c_1 & 0 & 0 & \ldots & c_{N-1} & c_0 \end{bmatrix}, \tag{9}$$

in which each row is a cyclic shift of the row above it.

Note that when working with circulant matrices it is convenient to number entries from 0 to *N*-1 rather than from 1 to *N*.

Every circulant matrix [*C*] of order *N* has eigenvectors [3]

$$\{X\}_p = \frac{1}{\sqrt{N}} \begin{Bmatrix} 1 \\ e^{-ip\theta.1} \\ e^{-ip\theta.2} \\ \vdots \\ e^{-ip\theta.q} \\ \vdots \\ e^{-ip\theta(N-1)} \end{Bmatrix} = \frac{1}{\sqrt{N}} \begin{Bmatrix} 1 \\ W_N^{1.p} \\ W_N^{2.p} \\ \vdots \\ W_N^{q.p} \\ \vdots \\ W_N^{(N-1).p} \end{Bmatrix} = \frac{1}{\sqrt{N}} \begin{Bmatrix} 1 \\ W_1^p \\ W_2^p \\ \vdots \\ W_q^p \\ \vdots \\ W_{N-1}^p \end{Bmatrix}, (p = 0, \ldots, N-1) \tag{10}$$

where

$$\theta = \frac{2\pi}{N} \tag{11}$$

is the angle between two neighbouring masses,

$$w_q = e^{-i\theta q} = w_N^q (q = 0, \ldots, N-1) \tag{12}$$

are complex "roots of unity" and

$$w_N = e^{-i\frac{2\pi}{N}} = e^{-i\theta} \tag{13}$$

is the primitive *N*-th root of unity.

The corresponding eigenvalues are

$$\omega_p^2 = \sum_{q=0}^{N-1} c_q e^{-i\frac{2\pi}{N}pq} = \sum_{q=0}^{N-1} c_q e^{-i\theta pq}. \tag{14}$$

For *N* even, the zeroth eigenvalue ω_0^2 and the so-called Nyquist eigenvalue $\omega_{N/2}^2$ are always real. For real symmetric circulant matrices, the remaining eigenvalues are real and come in pairs symmetric about $\omega_{N/2}^2$.

For the system shown in Fig.1 the eigenvalues are

$$\omega_p^2 = c_0 + c_1 w_N^p + c_{N-1} w_N^{(N-1)p}, \tag{15}$$

$$\omega_p^2 = \frac{k+2s}{m} - \frac{2s}{m}\cos\left(\frac{2\pi}{N}p\right), \ (p = 0, \dots, N-1). \tag{16}$$

The eigenvectors belonging to double eigenvalues are complex conjugate. Because any linear combination of the eigenvectors belonging to a repeated eigenvalue is also an eigenvector, the real and imaginary parts of the eigenvectors are themselves eigenvectors, and are usually termed as the "cosine" and "sine" modes.

The antisymmetric *cosine* mode corresponds to the first eigenvalue in a pair, and the symmetric *sine* mode corresponds to the second eigenvalue.

Instead of ordering the eigenvalues according to the index *p*

$$\omega_0^2, \omega_1^2, \omega_2^2, \dots\dots, \omega_{N-2}^2, \omega_{N-1}^2 \tag{17}$$

it is common practice to number them in increasing magnitude order as

$$\omega_0^2, \omega_1^2, \omega_{N-1}^2, \omega_2^2, \omega_{N-2}^2, \dots\dots, \omega_{N/2}^2. \tag{18}$$

Sometimes it is convenient to re-index the modes of vibration and the elements of modal vectors (masses *m*) from 1 to *N* (Fig. 1) [2].

$$\begin{aligned} \omega_p^2\big|_{p=0,1,2,\dots\dots,N-1} &= \lambda_r|_{r=1,2,\dots\dots,N} \\ \{X\}_p\big|_{p=0,1,2,\dots\dots,N-1} &= \{Y\}_r|_{r=1,2,\dots\dots,N} \\ \{X_q\}\big|_{q=0,1,2,\dots,N-1} &= \{Y_j\}\big|_{j=1,2,\dots\dots N} \end{aligned} \tag{19}$$

Numerical example

Consider the system from Fig.1 with the following numerical parameters

$$k = 10^4\ N/m\ ,\ s = k/10\ ,\ m = 1\ kg\ , N = 12. \tag{20}$$

The eigenvalues ordered as in (17) are

$$\omega_p^2 = 1.2 \cdot 10^4 - 0.2 \cdot 10^4\ cos\left(\frac{p\pi}{6}\right), \quad (p = 0, 1, \dots, 11) \tag{21}$$

i.e.

$$\begin{gathered} \lambda_1 = 1e^4,\ \lambda_2 = \lambda_{12} = 1.0268e^4,\ \ \lambda_3 = \lambda_{11} = 1.1e^4,\ \ \lambda_4 = \lambda_{10} = 1.2e^4, \\ \lambda_5 = \lambda_9 = 1.3e^4,\ \lambda_6 = \lambda_8 = 1.3732e^4,\ \lambda_7 = 1.4e^4. \end{gathered} \tag{22}$$

The eigenfrequencies are showed in the upper plot of Fig.2. In the lower plot they are ordered as in (18).
The mode shapes of the undamped system are shown in Fig.3 and Table 1. The deflection amplitudes are defined by the real *cosine* and *sine* modes [4]:

for antisymmetric modes

$$\{Y_j^A\}_1 = 1, \quad j = 1{:}\,12, \tag{23}$$

$$\{Y_j^A\}_n = \cos\left[\frac{n}{2}(j-1)\frac{\pi}{6}\right], \quad n = 2,4,6,8,10,12; \tag{24}$$

for symmetric modes

$$\{Y_j^S\}_n = -\sin\left[(12-\tfrac{n-1}{2})(j-1)\tfrac{\pi}{6}\right], \quad n = 3,5,7,9,11. \tag{25}$$

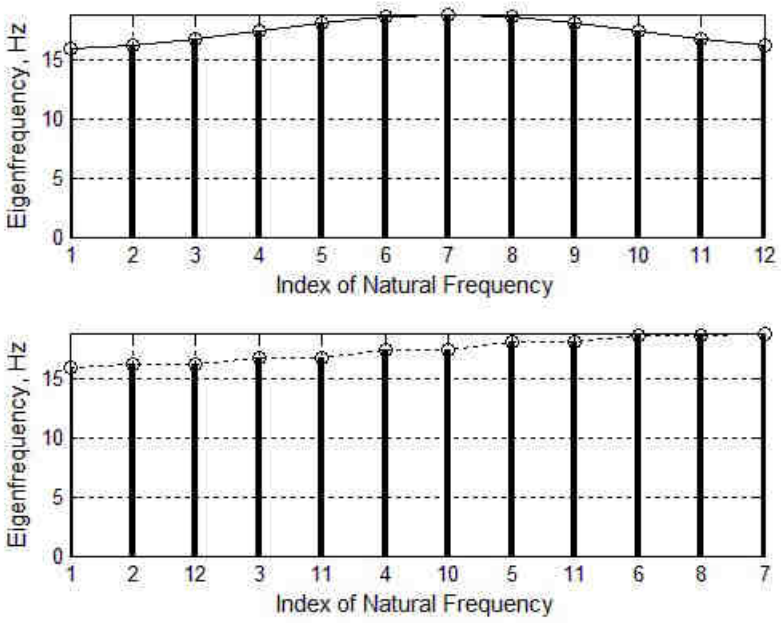

Fig. 2**.** The undamped natural frequencies.

By analogy with the mode shapes of bladed discs [5], it is possible to define "nodal diameters", i.e. lines connecting opposite points with zero displacement.
Except when $p = 0$ and $p = N/2 = 6$, there are pairs of mode shapes with the same shape but rotated relatively. The mode shape corresponding to the second of each pair of frequencies is rotated by an angle $\pi/2D$, where D is the number of "nodal diameters". Modes 2 and 3 are "1D" modes $(D = 1)$ in which the nodal diameter is rotated by 90^0. Modes 4 and 5 are "2D" modes $(D = 2)$, whose nodal diameters are rotated by 45^0. Modes 6 and 7 are "3D" modes $(D = 3)$, with nodal diameters rotated by 30^0 and so on (the "4D" modes 8 and 9 are rotated $22{,}5^0$, while the "5D" modes 10 and 11 are rotated 18^0).

A different plot of the mode shapes is presented in Fig. 4.

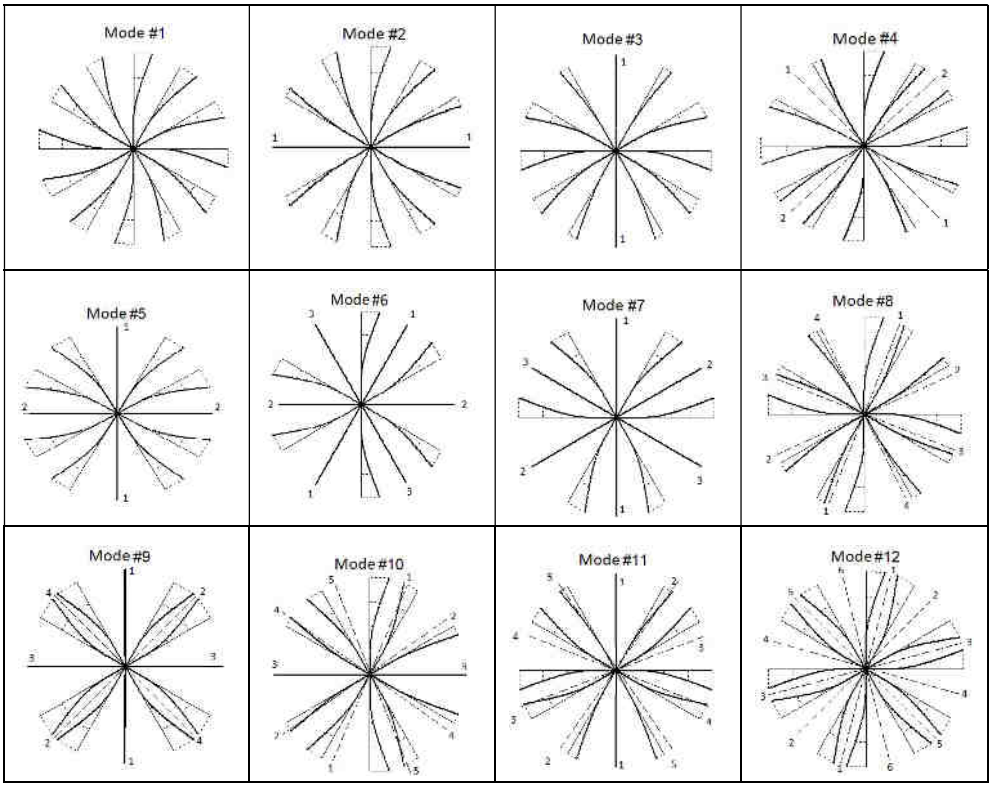

Fig. 3. The mode shapes of the undamped system.

Modes 3, 5, 7, 9, 11 are symmetric *sine* modes, while modes 2, 4, 6, 8, 10 are antisymmetric *cosine* modes. When $p = 0$ the sine shape vanishes and all masses have uniform displacements. When $p = 6$ every mass vibrates in anti-phase with its adjacent neighbours.

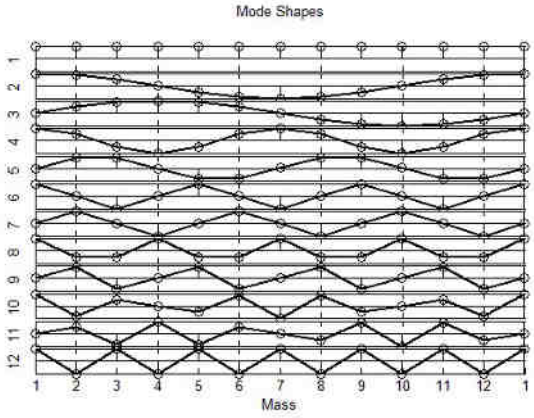

Fig. 4. Mode shapes of the undamped system

Table 1. Natural frequencies and mode shapes of the undamped tuned system

	Mode shape											
	1	2	3	4	5	6	7	8	9	10	11	12
Mass	Natural frequencies, Hz											
	15.91	16.127		16.692		17.435		18.146		18.650		18.83
	Displacement amplitude											
1	1	1	0	1	0	1	0	1	0	1	0	1
2	1	0.866	0.5	0.5	0.866	0	1	-0.5	0.866	-0.866	0.5	-1
3	1	0.5	0.866	-0.5	0.866	-1	0	-0.5	-0.866	0.5	-0.866	1
4	1	0	1	-1	0	0	-1	1	0	0	1	-1
5	1	-0.5	0.866	-0.5	-0.866	1	0	-0.5	0.866	-0.5	-0.866	1
6	1	-0.866	0.5	0.5	-0.866	0	1	-0.5	-0.866	0.866	0.5	-1
7	1	-1	0	1	0	-1	0	1	0	-1	0	1
8	1	-0.866	-0.5	0.5	0.866	0	-1	-0.5	0.866	0.866	-0.5	-1
9	1	-0.5	-0.866	-0.5	0.866	1	0	-0.5	-0.866	-0.5	0.866	1
10	1	0	-1	-1	0	0	1	1	0	0	-1	-1
11	1	0.5	-0.866	-0.5	-0.866	-1	0	-0.5	0.866	0.5	0.866	1
12	1	0.866	-0.5	0.5	-0.866	0	-1	-0.5	-0.866	-0.866	-0.5	-1

2.2. Undamped mass-mistuned system

A single mass of $0.1\ kg$ is attached to the mass $m = 1\ kg$ at $q = 0$. The natural frequencies and mode shapes of the mistuned system are presented in Table 2.

As expected [3], the double modes split into pairs of modes, one with a lower natural frequency, the other remaining essentially the same.

The mode corresponding to the unaltered frequency remains unchanged, but rotated such that one of the "nodal diameters" passes through the mistuning mass. The mode corresponding to the lower frequency has a distorted shape. The points of zero displacement amplitude are no more on a "nodal diameter". The half part containing the attached mass has smaller displacements compared with the other half [5].

Table 2. Natural frequencies and mode shapes of the mass-mistuned system

	Mode shape											
	1	2	3	4	5	6	7	8	9	10	11	12
	Natural frequency, Hz											
	15.73	16.02	16.13	16.57	16.69	17.30	17.43	18.02	18.15	18.54	18.65	18.80
Mass	Displacement amplitude											
1	1	0.575	0	0.832	0	0.860	0	0.818	0	0.652	0	0.289
2	0.626	0.246	0.5	0.034	1	-0.432	1	-0.859	1	-0.985	0.5	-0.485
3	0.395	-0.115	0.866	-0.793	1	-0.937	0	-0.115	-1	0.882	-0.866	0.659
4	0.254	-0.461	1	-0.957	0	0.265	-1	0.953	0	-0.405	1	-0.803
5	0.172	-0.747	0.866	-0.322	-1	0.984	0	-0.665	1	-0.243	-0.866	0.911
6	0.129	-0.934	0.5	0.582	-1	-0.089	1	-0.409	-1	0.788	0.5	-0.977
7	0.116	-1	0	1	0	-1	0	1	0	-1	0	1
8	0.129	-0.934	-0.5	0.582	1	-0.089	-1	-0.409	1	0.788	-0.5	-0.977
9	0.172	-0.747	-0.866	-0.322	1	0.984	0	-0.665	-1	-0.243	0.866	0.911
10	0.254	-0.461	-1	-0.957	0	0.265	1	0.953	0	-0.405	-1	-0.803
11	0.395	-0.115	-0.866	-0.793	-1	-0.937	0	-0.115	1	0.882	0.866	0.659
12	0.626	0.246	-0.5	0.034	-1	-0.432	-1	-0.859	-1	-0.985	-0.5	-0.485

2.3. Damped tuned system

To generate frequency response curves for the principal component analysis, *proportional* damping is added to the cantilevers $c = 0.1\ Ns/m$ and to the coupling springs $c_s = 0.01\ Ns/m$ of the system shown in Fig.1.

For proportional damping, knowing the real eigenvectors, the diagonal modal mass, stiffness and damping matrices are calculated as

$$[m_r] = [Y]^T[M][Y],\quad [k_r] = [Y]^T[K][Y],\quad [c_r] = [Y]^T[C][Y]. \tag{26}$$

wherefrom the undamped natural frequencies and modal damping ratios are obtained as

$$\omega_r^2 = k_r/m_r,\ \zeta_r = \frac{c_r}{2m_r\,\omega_r}. \tag{27}$$

Modal parameters of the proportionally damped tuned system are given in Table 3.

Table 3. Modal parameters of the damped tuned system.

Mode	Modal mass	Modal stiffness	Modal damping coefficient	Eigenvalue	Natural frequency, Hz	Modal damping ratio
1	12	$1.2 \cdot 10^5$	1.2	$1 \cdot 10^4$	15.9155	$0.5 \cdot 10^{-3}$
2	6	$0.6161 \cdot 10^5$	0.6161	$1.0268 \cdot 10^4$	16.1273	$0.5067 \cdot 10^{-3}$
3	6	$0.6161 \cdot 10^5$	0.6161	$1.0268 \cdot 10^4$	16.1273	$0.5067 \cdot 10^{-3}$
4	6	$0.66 \cdot 10^5$	0.66	$1.1 \cdot 10^4$	16.6923	$0.5244 \cdot 10^{-3}$
5	6	$0.66 \cdot 10^5$	0.66	$1.1 \cdot 10^4$	16.6923	$0.5244 \cdot 10^{-3}$
6	6	$0.72 \cdot 10^5$	0.72	$1.2 \cdot 10^4$	17.4346	$0.5477 \cdot 10^{-3}$
7	6	$0.72 \cdot 10^5$	0.72	$1.2 \cdot 10^4$	17.4346	$0.5477 \cdot 10^{-3}$
8	6	$0.78 \cdot 10^5$	0.78	$1.3 \cdot 10^4$	18.1465	$0.5701 \cdot 10^{-3}$
9	6	$0.78 \cdot 10^5$	0.78	$1.3 \cdot 10^4$	18.1465	$0.5701 \cdot 10^{-3}$
10	6	$0.8239 \cdot 10^5$	0.8239	$1.3732 \cdot 10^4$	18.6504	$0.5859 \cdot 10^{-3}$
11	6	$0.8239 \cdot 10^5$	0.8239	$1.3732 \cdot 10^4$	18.6504	$0.5859 \cdot 10^{-3}$
12	12	$1.68 \cdot 10^5$	1.68	$1.4 \cdot 10^4$	18.8315	$0.5916 \cdot 10^{-3}$

The modal damping ratios are of the order 0.05 to 0.06 percent and the damped natural frequencies are essentially equal to the undamped natural frequencies.

2.4. Diagrams of the Frequency Response Functions

FRF curves are shown as magnitude (log scale) versus frequency (linear scale) plots. Receptance Frequency Response Functions *FRFij* have been simulated for displacement at coordinate (mass) *i* produced by excitation at coordinate (mass) *j*. Overlaid curves of the contributing modes of vibration correspond to the respective term in the partial fraction format.

The function FRF11 is shown in Fig.5. Because the symmetric "*sine"* modes 3, 5, 7, 9, 11 have a node at the mass $j = 1$, they are not excited by a force applied at 1, and do not contribute to the total response. It is obvious that such a plot cannot reveal double modes.

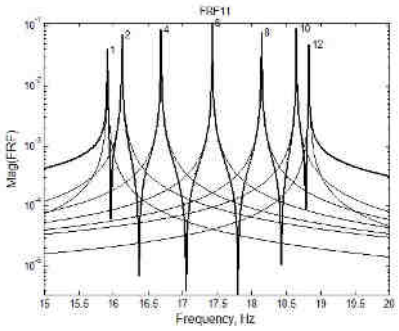

Fig. 5. Diagram of FRF11.

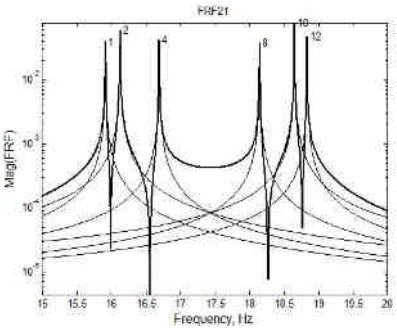

Fig. 6. Diagram of FRF21.

The FRF21 plot in Fig.6 has six peaks. Apart from modes 3, 5, 7, 9, 11 with a node at mass 1, the contribution of mode 6 is negligible, having a nodal point at mass 2.

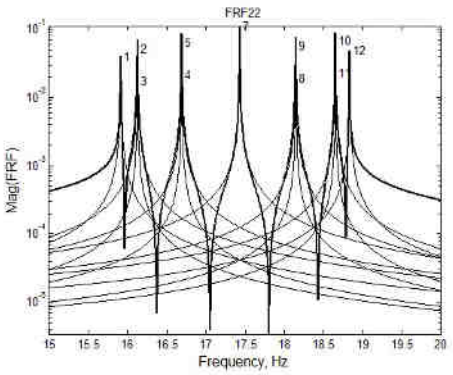

Fig.7. Diagram of FRF22.

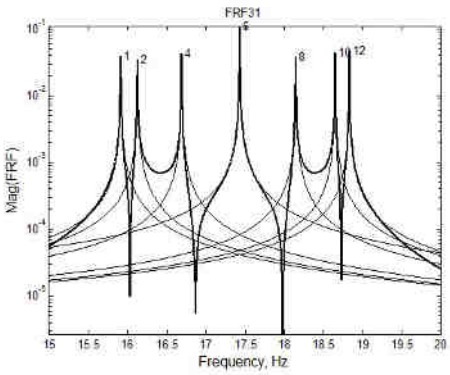

Fig. 8. Diagram of FRF31.

The magnitude plot of FRF22 is presented in Fig.7. Only the 6th mode is missing which exhibits a nodal point at mass 2. At four peaks, visual inspection of such a plot cannot detect the existence of double modes in the response. If the contribution of the other modes can be neglected, analysis by single degree of freedom techniques of such individual peaks of *direct* FRFs yields fairly good estimations of the modal parameters, because the sum of the partial fraction numerators of the two modes is independent of the mode shape.
The FRF31 plot from Fig.8 has seven peaks produced by seven modes, because the weakly excited modes 3, 5, 7, 9, 11 have a nodal point at mass 1, and mode 7 has a node at mass 3.

3. SVD of the compound FRF matrix

Consider a set of test data in the form of *N* complex valued Frequency Response Functions (FRFs) sampled at N_f frequencies, arranged columnwise in a Compound

Frequency Response Function (CFRF) matrix $[A] \in \mathbf{C}^{N_f xN}$. Each column contains the N_f frequency-dependent elements of an individual FRF, measured at a given output/input co-ordinate combination. Each row contains *N* complex FRF values measured at the same frequency.

The Singular Value Decomposition (SVD) of the CFRF matrix can be written

$$[A] = [U]\,[\Sigma]\,[V]^H = \sum_{i=1}^{N} \sigma_i \{u\}_i \{v\}_i^H = \sum_{i=1}^{N} \{A\}_i \qquad (28)$$

where $\{U\} \in \mathbf{C}^{N\,f\,xN}$ and $\{V\} \in C^{NxN}$ are the matrices of the left and right singular vectors, respectively, and the superscript *H* denotes the conjugate transpose (Hermitian). The singular values σ_i are arranged in non-increasing order of magnitude in the real diagonal matrix $[\Sigma]$.

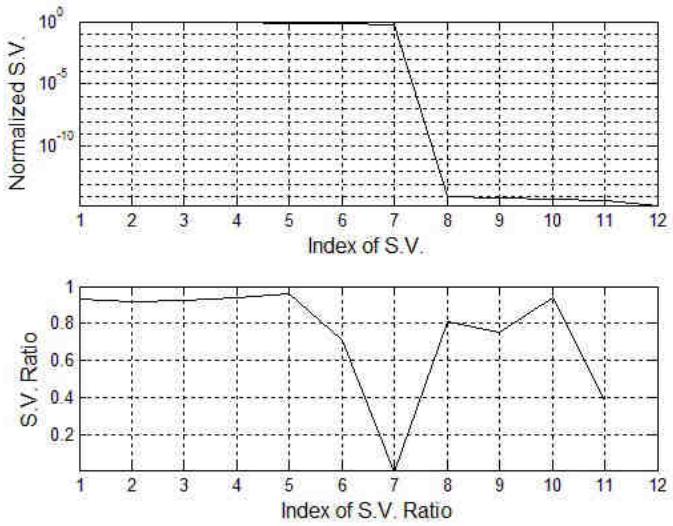

Fig.9**.** Diagrams of the singular values of the CFRF matrix, excitation in 2 and response in 1-12

Because the left and right singular vectors have unit length, the amplitude information is contained in the singular values. The SVD decomposes the CFRF matrix into a sum of rank-one matrices $\{A\}_i = \sigma_i \{u\}_i \{v\}_i^H$ of the same size as $[A]$. Each singular value is equal to the Frobenius norm of the associated $\{A\}_i$ matrix

$$\sigma_i = \|\{A\}_i\|_F \qquad (29)$$

and can be considered as a measure of its energy content.

In the upper plot in Fig.9, magnitudes of the singular values are plotted on a logarithmic scale, normalized to the largest singular value. The sudden drop in the curve after the seventh singular value indicates that there are seven important modes in the frequency band. This conclusion is supported by the plot of the ratio of successive singular values, which shows a distinct minimum at index 7.

The right singular vectors (RSV), $\{v\}_i$, describe the spatial distribution of the energy contained in the FRF set.

3.1 The U-Vector Mode Indicator Function (UMIF)

The left singular vectors (LSV)

$$\{u\}_i = \frac{1}{\sigma_i} \sum_{j=1}^{N} v_{ji} \{a\}_j \qquad (30)$$

contain the frequency distribution of the energy, being linear combinations of the original FRFs that form the columns of $[A]$. The LSV are mutually (pairwise) orthogonal vectors, so they are linearly independent. Their plot versus frequency is the *U-Vector Mode Indicator Function* (UMIF) [6]. The UMIF has peaks at the damped natural frequencies.

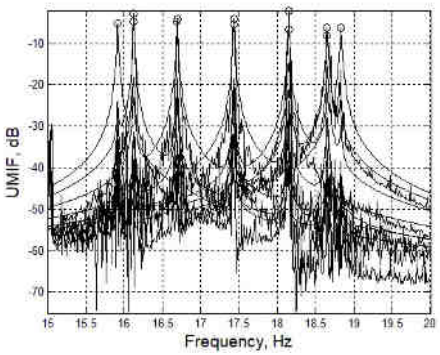

Fig.10. UMIF.

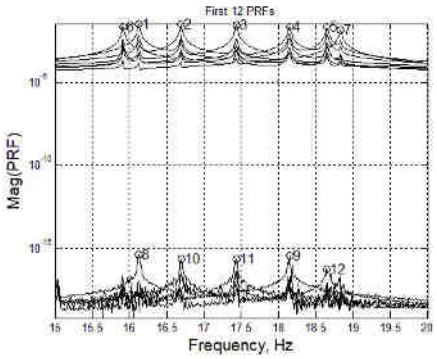

Fig.11. Diagram of PRFs.

The UMIF shown in Fig.10 is based on 12 noise free receptance FRFs calculated as responses at masses 1 to 12 due to excitation at mass 2. It contains 12 curves exhibiting peaks at the natural frequencies. In order to better locate the modes, the peaks are marked by circles. This is useful especially for noise polluted data.

3.2 Principal Response Functions (PRFs)

The SVD of the CFRF matrix is used to define Principal Response Functions (PRFs). Plots of PRFs versus frequency have peaks at the natural frequencies and can be used to locate double modes [7].

The Principal Response Functions, $\{p\}_i$, defined as the LSVs scaled by the respective singular values, are linear combinations of the original FRFs, $\{a\}_j$:

$$\{p\}_i = \sigma_i \{u\}_i = [A]\{v\}_i = \sum_{j=1}^{N} v_{ji} \{a\}_j. \qquad (31)$$

The PRF plot from Fig.11 is determined for the same input/output conditions as the UMIF plot in Fig.8. Here the 7 important modes are clearly separated from the 5 modes with low energy. The scaling of the PRFs by the singular values makes them less appropriate for use as modal indicators.

3.3 The Componentwise Mode Indicator Function (CoMIF)

The Componentwise Mode Indicator Function is defined [8] by vectors

$$\{CoMIF\}_i = \{1\} - \{u\}_i \otimes \{u\}_i^* \tag{32}$$

computed as the difference between a column vector of ones and the Hadamard product of the left singular vectors. In equation (32) the star superscript denotes the complex conjugate.

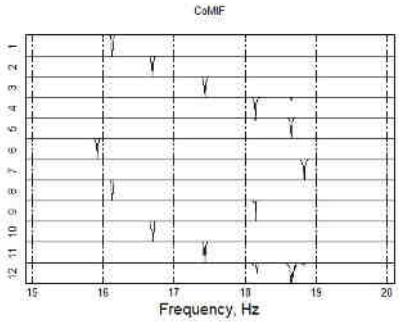

Fig.12. CoMIF with subplots

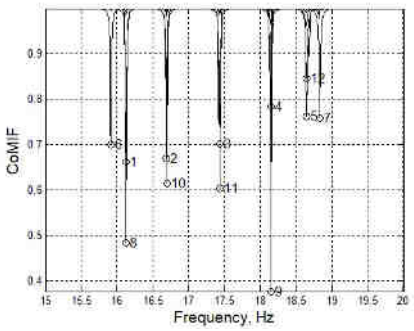

Fig.13. CoMIF with overlaid curves

In the CoMIF plot, the number of curves is equal to the rank of the CFRF matrix. Each curve has a local minimum at a damped natural frequency, with the deepest trough at the natural frequency of the corresponding dominant mode.

The CoMIF plot with individual curves displayed separately in subplots is shown in Fig.12 for the same input/output conditions as the PRF plot of Fig.11: input at 2 and output at 1 to 12, with noise free data. Subplots correspond to individual CoMIFs with the index shown on the left. A cursor is provided to better locate the damped natural frequencies.

The CoMIF plot with overlaid curves is shown in Fig.13. In order to better locate the natural frequencies, the lowest trough of each curve is marked by a circle with the index shown next to the right. This is useful especially in the case of lightly damped systems with repeated natural frequencies. Both CoMIF plots clearly locate all 12 modes of vibration, despite the single point excitation in a system with double modes.

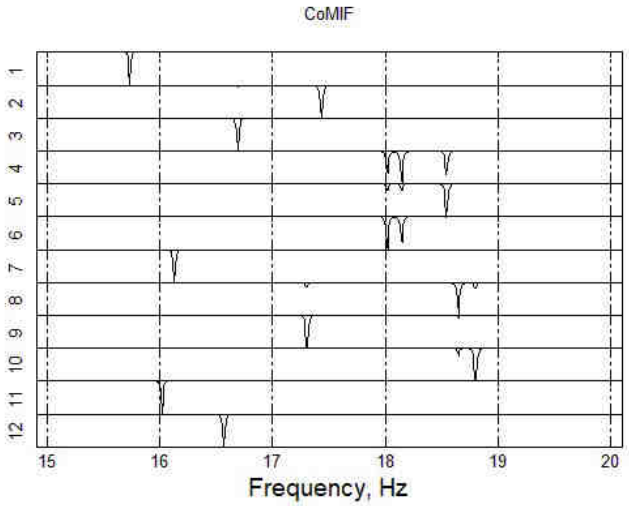

Fig. 14. CoMIF of mistuned system.

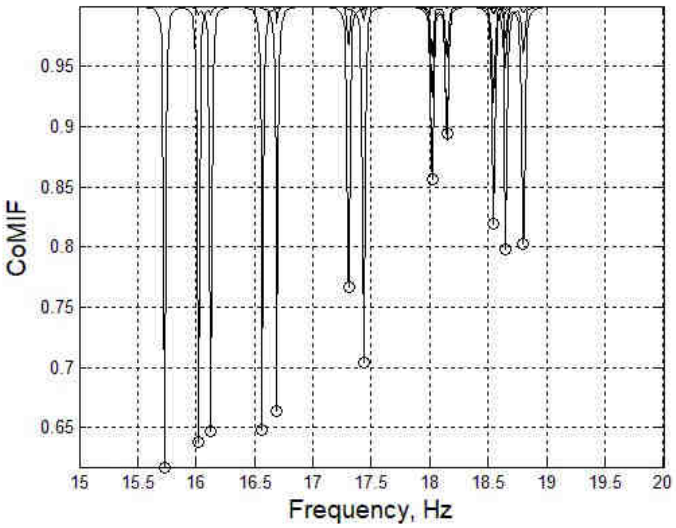

Fig. 15. Overlaid CoMIF of mistuned system.

For comparison, Figs.14 and 15 show the CoMIF plots for the damped mass-mistuned system, based on 12 FRFs with input at 2, output at 1 to 12 and noise free data. They illustrate how the double modes are split by mistuning. In Fig.14 the *damped* natural frequencies are located by the deepest trough of each subplot.

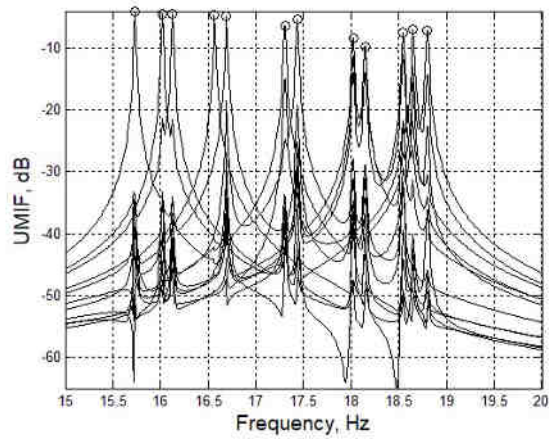

Fig. 16. UMIF of mistuned system .

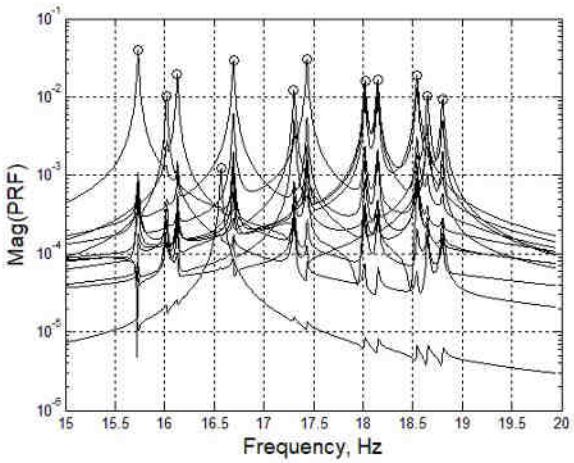

Fig. 17. PRF plot of mistuned system.

Note that the above presented CoMIF plots are based on noise free FRFs obtained with single point excitation. If the pattern of CoMIF curves is not so clear, it is recommended to change the excitation point or use excitation in two points.
The UMIF and PRF plots for the damped mistuned system are presented in Figs.16 and 17, based on 12 FRFs with input at 2, output at 1 to 12 and noise free data. On both diagrams all 12 natural frequencies are clearly located.

4. Concluding remarks

To determine the number of modes present in a frequency range, the Mode Indicator Functions (MIFs) in current use are based on the stepwise analysis of rectangular FRF matrices, one frequency at a time. To locate close modes, such

MIFs require FRFs measured at a number of input points equal to the multiplicity of eigenfrequencies. Examples are the Complex Mode Indicator Function (CMIF) and the Multivariate Mode Indicator Function (MMIF) [7]. Their plots have as many curves as the number of references.
The mode indicators UMIF and CoMIF, based on the left singular vectors of a matrix encompassing all measured FRFs as columns, can reveal double modes even for single reference. This was illustrated for a cyclic lumped parameter 12-mass system using simulated FRF data.

References

[1] McCallion H., *Vibration of Linear Mechanical Systems*, Longman, London, 1973.
[2] Olson B., Shaw S., Shi Chenzhi, Pierre Ch., Parker R., *Circulant Matrices and Their Application to Vibration Analysis*, Applied Mechanics Review, vol. 66, no. 4, 2014 <hal-01378829>.
[3] Gray R.M., *Toeplitz and Circulant Matrices*: *A review*, Now Publishers Inc., Boston, 2006.
[4] Wu Gaofeng, *Free Vibration Modes of Cyclic Assemblies with a Single Disordered Component,* J. Sound Vibration, **165**, 3, 1993, p. 563-570.
[5] Midturi S., Stange W.A., Reed J.D., *Modal Response of a Rotating Disk Assembly*, Proceedings of Int. Modal Analysis Conf. IMAC-5, London, p. 226-233, 6-9 April 1987.
[6] Radeş M., *Displays of Vibration Properties*, in *Encyclopedia of Vibration* (S. Braun, D. Ewins and S.S. Rao, eds.), Academic Press, London, **1**, 2001, p. 413-431.
[7] Radeş M., *Performance of Various Mode Indicator Functions*, Shock and Vibration, U.S.A., **17**, Nos. 4-5, June 2010, p. 473-482
[8] Radeş M., Ewins D.J., *The Componentwise Mode Indicator Function*, Proceedings of IMAC-19 Conference on Structural Dynamics, Kissimmee, Florida, 2001, p. 903-908.
[9] Radeş M., *A Comparison of Some Mode Indicator Functions,* Mechanical Systems and Signal Processing, **8**, 4, 1994, p. 459-474.